ISTITUTO NAZIONALE DI FISICA NUCLEARE

Sezione di Catania

INFN/BE-87/1
19 Febbraio 1987

G. Lanzanò, A. Pagano, R.A. Dayras and F. Gadi:

A SIMPLIFIED GEOMETRICAL APPROACH TO THE FAST ABRASION MODEL

Servizio Documentazione
dei Laboratori Nazionali di Frascati

INFN - Istituto Nazionale di Fisica Nucleare
Sezione di Catania

INFN/BE-87/1
19 Febbraio 1987

A SIMPLIFIED GEOMETRICAL APPROACH TO THE FAST ABRASION MODEL.

G. Lanzanò, A. Pagano
ISTITUTO NAZIONALE DI FISICA NUCLEARE
Corso Italia, 57 95129 Catania, ITALY

R.A. Dayras, F. Gadi
DPhN/BE, CEN Saclay, 91191 Gif/Yvette Cedex, FRANCE

ABSTRACT

An approximated geometrical approach to the fast abrasion model is proposed, in order to get simple analytical formulas for the most common physical observables measurable in either inclusive and exclusive experiments. The results obtained are satisfactorily compared with either the predictions of the extended abrasion model of R.A. Dayras and the recent experimental results obtained at intermediate energies.

1. INTRODUCTION

With the advent of new accelerators working at intermediate energies, many experiments have been accomplished, aimed to study the reaction mechanism involved in this transitional energy region. The projectile fragmentation is by far the most important of the processes involved, accounting for ≃ 80% of the reaction cross section [1] .

The abrasion-ablation model, typical of higher relativistic energies [2] , has been widely used in computing abrasion cross sections and prefragment excitation energies [3] . Recently R.A.Dayras has extended the abrasion model, in order to include also kinematical effects [4] . However, concerning the first step of this model, i.e. the abrasion stage, no simple analytical formulae exist for computing relevant physical quantities, as cross sections or excitation energies of the produced prefragments. Approximate formulae have been used (but not described) in ref. [5] , based on Swiatecki's unpublished notes [6] . They are available in the appendix of ref. [7] .

In this paper we present a simple analytical method to obtain approximate formulae for relevant physical quantities whenever the fast abrasion model is applied either in inclusive or exclusive experiments. The validity of the model is discussed, and the results are compared either with the "exact" predictions of the extended abrasion model [4] and some recent experimental results.

2. THE MODEL

In the fast abrasion model it is assumed that the overlap region between target and projectile is sheared away to form a hot zone of nuclear matter, the "participants", whereas the remaining parts of the projectile and target, the "spectators", are only slightly perturbed. In the frame of this model, to compute the prefragments abrasion cross-section and their excitation energy implies the knowledge of the volume and the surface of the two abraded nuclei as a function of the impact parameter b.
Recently Dayras et al. have solved "exactly" this problem by an integration method, supposing, as customary, the surfaces and the volumes of the two abraded nuclei generated by the intersection between a sphere and a cylinder. In the following we shall develop the fast abrasion model, as outlined above, introducing the simplifying approximation that the surfaces of the two abraded nuclei can be treated as spherical segments.

Let us suppose the two colliding nuclei spherical with a uniform distribution of nucleons inside, being A_P and A_T the projectile and target masses. After the abrasion process a projectile-like fragment (PLF) and a target-like fragment (TLF), generally excited, with mas

ses respectively A_{PF} and A_{TF} are produced (the "spectators"). In the same process a zone of nuclear matter, with mass A_{PT} and highly excited, is assumed to be formed, generated from the overlapping of the participant zones of the two nuclei, with masses respectively $(A_P-A_{PF})$and(A_T-A_{TF}),see Fig.1a. If now we suppose that the shape of the two abraded fragments can be approximated by a spherical segment, by looking at Fig.1a we can introduce the useful parameter $x=\cos\theta_P=1-\frac{h}{R_P}$, being $R_P= r_0 A_P^{1/3}$the projectile radius. In the same way we define a parameter $x_T=\cos\theta_T=1-\frac{h}{R_T}$ relative to the target-like fragment. x is depending only on the ratio A_{PF}/A_P, as can be shown by taking the exact cardanic solution of the cubic equation

$$x^3-3x + 2\left(2\frac{A_{PF}}{A_P} - 1\right) = 0 \qquad (1)$$

relating x to the projectile-like fragment mass A_{PF}.

For $0<A_{PF}<A_P$, x ranges between -1 and +1, vanishing for $A_{PF}/A_P=1/2$, and the unique solution of eq.(1) is given by:

$$x = 2\cos\left[\frac{\arccos\left(1-2\cdot\frac{A_{PF}}{A_P}\right)}{3} + \frac{4}{3}\pi\right] \qquad (2a)$$

The trend of x as a function of the ratio $A_{PF}/A_P$is given in Fig.2. In the same way we obtain for the target-like fragment:

$$x_T = 2\cos\left[\frac{\arccos\left(1-2\cdot\frac{A_{TF}}{A_T}\right)}{3} + \frac{4}{3}\pi\right] \qquad (2b)$$

The impact parameter b is related in a linear way to x or x_T, and is given simply by:

$$b = R_T + R_P x = R_P+R_T x_T \qquad (3)$$

being $R_T=r_0A_T^{1/3}$ the target radius.

The projectile and target abraded surfaces are given respectively by:

$$S_{PF} = \pi r_o^2 A_P^{2/3}(1-x^2) \tag{4a}$$

and

$$S_{TF} = \pi r_o^2 A_T^{2/3}(1-x_T^2) \tag{4b}$$

Finally the dependence of A_{PF} on x (or A_{TF} on x_T) is given simply by :

$$\frac{A_{PF}}{A_P} = -\frac{1}{4}x^3 + \frac{3}{4}x + \frac{1}{2} \tag{5a}$$

and

$$\frac{A_{TF}}{A_T} = -\frac{1}{4}x_T^3 + \frac{3}{4}x_T + \frac{1}{2} \tag{5b}$$

respectively.

3. RESULTS AND DISCUSSION

In this paragraph some predictions of the model will be shown about some physical quantities measurable either in inclusive or exclusive experiments, especially in the domain of intermediate energies.

3a. INCLUSIVE EXPERIMENTS

Energy spectra, angular distributions and absolute cross-sections for production of projectile-like fragments are the most common phyisical quantities measured in inclusive experiments. They are affected by the ablation stage following the abrasion process, so that in the following calculation we will refer to the projectile (or target)-like fragments before the ablation stage (the so-called "prefragments" or "primary fragments").

i) Abrasion cross-section

The cross-section for the production of a fragment of mass A_{PF} is calculated as:

$$\frac{d\sigma}{dA_{PF}} = \frac{d\sigma}{db} \cdot \frac{db}{dx} \cdot \frac{dx}{dA_{PF}}$$

where $d\sigma = 2\pi b db$ and b and x are given by relations (3) and (2a) respectively. The result is simply:

$$\frac{d\sigma}{dA_{PF}} = \frac{2}{3}\pi \cdot r_o^2 A_P^{-1/3} \left[\left(\frac{A_T}{A_P}\right)^{1/3} + x \right] \cdot \frac{\sqrt{4-x^2}}{\sqrt{\frac{A_{PF}}{A_P}\left(1-\frac{A_{PF}}{A_P}\right)}} \qquad (6)$$

In the fig.3 the predictions of equation (6) are compared with the exact numerical results of the extended abrasion model[4] for projectile-like fragments issued from ^{40}Ar induced reactions on various targets. The accord is in general very good and discrepancies are contained within 10% for $\frac{A_{PF}}{A_P} \gtrsim \frac{1}{2}$. The only parameter entering in formula (6) is r_o, that has been fixed at 1.36 fm for the curves shown in Fig.3. The comparison with the experimental data is in general not straightforward as the ablation stage or the presence of transfer-like processes (especially for values of A_{PF} near A_P) can modify substantially the trend of Fig.3. (See for instance ref[1,4]). In this regard it would be more interesting to compare the dependence of eq.(5) on x or A_T for reactions induced by the same beam relatively to a fixed target of mass A_{TO}. We can calculate $d\sigma/dA_{PF}$ as given by (6) for A_T and A_{TO}, and then we make the ratio R. We obtain:

$$R = \frac{d\sigma/dA_{PF}(A_T)}{d\sigma/dA_{PF}(A_{TO})} = \frac{\left(\frac{A_T}{A_P}\right)^{1/3} + x}{\left(\frac{A_{TO}}{A_P}\right)^{1/3} + x} \qquad (7)$$

This ratio is independent of the chosen value of r_o and its trend as a function of A_{PF}/A_P is comparable with the experimental data, as shown in ref[1,4] for the reactions $^{40}Ar+^{27}Al$ and $^{40}Ar+^{nat}Ti$ at 44 MeV/u. We have reported in Fig.4 the ratio R as a function of the target mass A_T, for a fixed value of the projectile-like mass A_{PF}=30 and relatively to a target mass A_{TO}=27. The experimental values shown have been extracted from various ^{40}Ar induced reactions at intermediate energies; as specified in the caption of the same figure. A value of 70 mb has been used for the production cross section of the projectile-like mass 30 in the reaction $^{40}Ar+^{27}Al$ at 44 MeV/u. An error of 15% has been assumed for all the reported experimental points. The trend of the experimental points

is fairly well reproduced by the relation (7).

ii) Energy damping

The main features of the PLF's energy spectra observed at intermediate energies can be resumed as follows: the maximum of the spectrum is located at an energy slightly lower than the one corresponding to the beam velocity, its width increasing as the PLF's mass is decreasing, and reaching a saturation value near $A_{PF}/A_P \simeq \frac{1}{2}$, the shape of the spectrum being asymmetric with a queue at the lower energy side. As an example in Fig.5 is shown the energy spectrum for the PLF ^{31}P detected at 2.5° in the reaction $^{40}Ar + ^{nat}Ti$ at 44 MeV/u, the arrow indicating the ^{31}P energy corresponding to the beam velocity.

It is unclear at this moment the origin of this asymmetry nor the widening of the spectrum for decreasing values of A_{PF}, and one possible explanation will be given in the following subsection. On the contrary the observed energy damping of the spectra is well expected, especially in this intermediate energy region. In fact let us consider the energy necessary to remove a fragment from the projectile in order to produce the projectile-like fragment of mass A_{PF}. In the framework of the abrasion model this separation energy con be easily calculated as:

$$E_{S,P} = 2\gamma S_{PF}$$

where $\gamma \simeq 0.95$ MeV/fm^2 is the nuclear surface tension coefficient and S_{PF} is the area of the flat abraded projectile surface. By using relation (4a) we obtain:

$$E_{S,P} = 2\gamma\pi r_o^2 A_P^{2/3} \cdot (1-x^2) \qquad (8)$$

Consequently the projectile-like fragment energy is shifted from $E_P \cdot A_{PF}/A_P$ to the value:

$$E_{PF} = E_P \cdot \frac{A_{PF}}{A_P} - 2\gamma\pi r_o^2 A_P^{2/3} \cdot (1-x^2) \qquad (9)$$

as first obtained, by the same method, in ref.[12].

We expect that the subsequent ablation stage does not change significantly the trend of eq.(9). In Fig.6 the observed experimental energy shift is reported as a function of A_{PF} for the most abundant isotopes and for the near projectile isotopes (S,Cl,Ar). The parabolic behaviour of eq.(8) with r_o=1.2 fm fits fairly well the experimental data, especially for $20 \leq A_{PF} \leq 36$.

For $A_{PF} \geq 36$ the observed energy shift is lower than the calculated one. This fact is generally interpreted as due to the predominance, in this mass region, of transfer processes[13].

In a same manner we can deduce the corresponding separation energy for the abraded target, that is given by

$$E_{S,T} = 2\gamma\pi r_o^2 A_T^{2/3} \cdot (1-x_T^2) \qquad (10)$$

We assume that the abrasion of the target is made at the expense of the energy of the participant fragment abraded from the projectile, with mass $A_P - A_{PF}$. Consequently the e-

nergy of this fragment is shifted to the value:

$$E_{P-PF} = E_P \cdot \frac{(A_P - A_{PF})}{A_P} - 2\gamma\pi r_o^2 A_T^{2/3} \cdot (1-x_T^2) \qquad (11)$$

iii) Prefragment excitation energy

Very little has been done experimentally to the aim of having some insight on the primary fragment excitation energy. Only recently an experiment of Gomez del Campo et al.[14,20] has evidenced that the prefragments issued from the reaction ^{40}Ar+Ge at 44MeV/u carry away only little excitation energy, in accord with a fast abrasion model calculation. The knowledge of the prefragment excitation energy is very important, as it influences directly the ablation stage and hence many physical observables.

In the framework of the abrasion model the excitation energy of the abraded fragment can be calculated as the difference of surface between the abraded fragment of mass A_{PF} and a spherical fragment of the same mass. The expressions that we obtain for the projectile and target abraded fragments of mass respectively A_{PF} and A_{TF} are the following:

$$E^*_{PF} = 4\gamma\pi r_o^2 A_P^{2/3} \cdot \left[\frac{3+2x-x^2}{4} - \left(\frac{2+3x-x^3}{4}\right)^{2/3} \right] \qquad (12a)$$

and

$$E^*_{TF} = 4\gamma\pi r_o^2 A_T^{2/3} \cdot \left[\frac{3+2x_T-x_T^2}{4} - \left(\frac{2+3x_T-x_T^3}{4}\right)^{2/3} \right] \qquad (12b)$$

respectively. As in our approximated model the abraded surfaces are assumed flat, we expect a marked difference between the prediction of relations (12a,b) and the results of the extended abrasion model. This comparison is made in Fig.7 for the projectile-like fragments issued from the reaction ^{40}Ar+^{48}Ti, and it is evident that the results of eq.(12a) are systematically lower than the one predicted by ref.[4] on the average by a factor 1.6.

As an example of physical quantities influenced by particle evaporation from excited fragments, let us consider the width of the experimental energy (or momentum) spectra.

If we restrict ourselves in the analysis of the higher energy side of the spectrum, to say starting from 80% of the maximum on the left, we can fit it by a gaussian[4], whose width shows a typical dependence on A_{PF}, very similar to the trend of the separation energy ΔE shown in Fig.6. We suggest that this broadening of the spectrum with the decreasing projectile-like mass, is due to the particle evaporation, which becomes more substantial as the excitation energy increases. More than one primary fragment with different excitation energy and having suffered a different energy damping in the abrasion process can contribute, with a different weight, to the observed experimental spectrum. Besides that, especially at small Laboratory angles, emitting one particle in the

forward or backward direction makes the velocity of the remaining nucleus to change by a significative amount, as observed at low incident energy [15]. In this particular case, i.e. emitting one particle in forward(0°)or backward(180°)direction,it is easy to show that the change in momentum is given by:

$$\Delta P_{(A_{PF}-a)} = 86.3(\mathrm{MeV/c})\cdot\sqrt{\frac{a(A_{PF}-a)}{A_{PF}}\cdot(E^{*}_{PF}-Q)} \qquad (13)$$

where $86.3\,(\mathrm{MeV/c})=2\sqrt{2\cdot 931.478}$, A_{PF} is the mass of the primary fragment, E^{*}_{PF}-Q is the relative kinetic energy between the residual fragment of mass $(A_{PF}-a)$ and the emitted particle of mass a. All these factors together with the fact that E^{*}_{PF} -Q too has a certain statistical distribution, contribute to broaden the energy spectrum. Accurate statistical calculations are needed to ascertain this hypothesis, together with a good knowledge of the excitation energy and angular momentum carried away by the primary fragments. As a coarse approximation relation (13) gives an idea of the momentum width with the projectile-like fragment mass A_{PF}. In fact, supposing E^{*}_{PF} -Q on the average constant as a function of A_{PF}, reminding that as A_{PF} decreases E^{*}_{PF} increases, the number of evaporated particles is growing with E^{*}_{PF} , so that we have to sum quadratically more contributions given by relation (13), all having the same factor 86.3MeV/c,and the resulting dispersion is assuming a trend similar to the familiar one of the Goldhaber law [16]. In this picture the emphasized constant σ_0 of the Goldhaber law reduces to the trivial value $2\sqrt{2\cdot 931.478}$ more adherent to the experimental value of ≈ 87 MeV/c observed at intermediate energies. Finally we want to stress the fact that relation (13), because of the term E^{*} -Q, is able to predict eventual structures in the width for isotopes having the same mass but different charge, as observed experimentally [4,8].

3b. EXCLUSIVE EXPERIMENTS

The knowledge of the reaction mechanism often requires more sophisticated or exclusive experiments, in which the correlation between two or more meaningful physical observables is measured. In this subsection we will try to get from the model some useful correlation formulas, as mass-mass or mass-angle correlations.

i) Mass-mass correlations

Looking at Fig.1a it is clear that the clean-cut abrasion model predicts well defined correlations between the projectile-like fragment mass and the mass of the target-like fragment or the fire-ball. To get this correlation we observe that for a given impact parameter b,x and x_T are bound by relation (3) so that we can express x_T as a function of x, and put it in eq.(5b), obtaining for the correlation A_{TF}-A_{PF}:

$$\frac{A_{TF}}{A_T} = \frac{1}{2} + \frac{3}{4}\left[1 - \left(\frac{A_P}{A_T}\right)^{1/3} \cdot (1-x)\right] - \frac{1}{4}\left[1 - \left(\frac{A_P}{A_T}\right)^{1/3} \cdot (1-x)\right]^3 \qquad (14)$$

where x is bound to A_{PF}/A_P by means of relation (2a). This correlation function depends only on the ratio $(A_P/A_T)^{1/3}$ and reduces to $A_{TF}/A_T = A_{PF}/A_P$ for $A_P/A_T = 1$. Its trend, for $A_{PF}/A_P \geq \frac{1}{2}$, is nearly linear and can be approximated by the following expression:

$$\begin{cases} A_{PF}/A_P \simeq m\,(A_{TF}/A_T) + n \\ m \simeq 1.577\,(A_T/A_P)^{1/3} - 0.577 \\ n \simeq 1 - m \end{cases} \qquad (15)$$

Finally let us calculate the mass of the fire-ball associated to a given projectile fragment A_{PF}. Observing that this mass A_{PT} is given by $A_{PT} = A_P + A_T - A_{PF} - A_{TF}$, we have:

$$A_{PT} = \frac{A_P}{4}\left\{2x^3 - 3\left[1 - \left(\frac{A_T}{A_P}\right)^{1/3}\right]x^2 - 6\left(\frac{A_T}{A_P}\right)^{1/3} x + 3\left(\frac{A_T}{A_P}\right)^{1/3} + 1\right\} \qquad (16)$$

In Fig.8 the masses A_{PF}, A_{TF} and A_{PT} emerging from the reaction $^{40}Ar + ^{27}Al$ are reported as a function of the "reduced impact parameter" x and compared with the prediction of ref.[4]. The trends of the two curves are very similar for the three fragments, and the agreement between them is expected to improve for reactions in which the projectile is smaller than the target. A much better agreement with the extended abrasion model we find in the correlation function as shown as an example, in Fig.9, where the correlation function $A_{PF} - A_{TF}$ is reported for the reaction $^{40}Ar + ^{27}Al$ and compared with the prediction of ref.[4]. Also shown in the same figure is the experimental mass correlation observed at 44 MeV/u[17]. On the average the experimental behaviour is reproduced fairly well, suggesting that yet at this energy the fast abrasion mechanism is setting in. More difficult to interprete are the very large widths accompanying this correlation, probably related to the ablation stage and/or to mean field residual effects.

No experimental data exist for the mass correlation between projectile-like fragments and fireball. Following relation (16) A_{PT} increases as A_{PF} decreases. However, due to its very high excitation energy, the fire-ball is expected to explode or to evaporate many particles. In this hypothesis the multiplicity of the light particles emerging from the overlap zone would increase as the projectile-like mass decreases. In this regard an attempt has been made[18] for the reaction $^{40}Ar + ^{27}Al$ at 44 MeV/u to relate the differential α particles multiplicity at +25° with the coincident projectile-like mass detected at +3.1°. Surprisingly the experimental results are in good agreement with the prediction of eq.(16), as shown in Fig.10, suggesting that the number of participant nucleons increases as the mass of the projectile-like fragments decreases. However such a conclusion may be premature without a more detailed knowledge of the correlations between light particles and projectile fragments, as the yield of particles at one angle

depends strongly on the angular distribution of the emitting primary fragments.

ii) Angular and kinematic correlations

The study of angular and kinematic correlations between projectile and target-like fragments constitute a very important tool to get a deeper knowledge on the reaction mechanism. To get these correlations from our model, let us look at Fig.1b), where the reaction scheme is reported. In the Laboratory system a projectile-like fragment of mass A_{PF} is emerging from the reaction at an angle θ_{PF} with respect to the beam direction, and with a velocity $v_{PF} = \sqrt{2E_{PF}/A_{PF}}$, where E_{PF} is given by relation (9). To know the angle - θ_{TF} and the velocity v_{TF} of the recoiling target-like fragment, we make the assumption that the fire-ball is emitted in the forward beam direction and that its momentum $A_{PT}v_{PT}$ in the Lab. system is given approximately by:

$$A_{PT}v_{PT} \simeq (A_P - A_{PF})v_{P-PF} \qquad (17)$$

where $v_{P-PF}=\sqrt{2E_{P-PF}/(A_P-A_{PF})}$ is the velocity of the projectile participants and is assumed to be shifted from the beam velocity by an amount corresponding to the separation energy necessary to abrade the target, as given by equation (11). By linear momentum conservation we have:

$$A_{PF}v_{PF}\cos\theta_{PF}+A_{PT}v_{PT}+A_{TF}v_{TF}\cos\theta_{TF} \simeq A_Pv_P$$

$$A_{PF}v_{PF}\sin\theta_{PF} - A_{TF}v_{TF}\sin\theta_{TF} \simeq 0$$

and putting $P_P=A_Pv_P$, $P_{PF}=A_{PF}v_{PF}$, $P_{P-PF}=(A_P-A_{PF})v_{P-PF}$, we get for the recoiling angle θ_{TF}:

$$\theta_{TF} = \text{arctg}\left[\frac{P_{PF}\sin\theta_{PF}}{P_P-P_{PF}\cos\theta_{PF}-P_{P-PF}}\right] \qquad (18)$$

and for the target-like fragment velocity:

$$v_{TF}=\sqrt{\frac{(P_P-P_{PF}\cos\theta_{PF}-P_{P-PF})^2+P_{PF}^2\sin^2\theta_{PF}}{A_{TF}^2}} \qquad (19)$$

The prediction of relation (18) is compared with the results of the extended abrasion model and with the experimental results[17] for the reaction $^{40}Ar+^{27}Al$ at 44 MeV/u in Fig.11. The agreement with both the experimental points and the results of ref.[4] is very satisfactory.

Finally the target-like velocities predicted by (19) are very low and growing with decreasing target-like mass in excellent accord with the existing data for the $^{40}Ar+^{27}Al$

reaction at 44 MeV/u[19,20].

4. CONCLUSION

We have attempted to give an overview on the main features of the fragmentation process at intermediate energy, studied either by means of inclusive and exclusive experiments. The extended version of the fast abrasion model, including kinematical effects, is able to account for most of the observed features. The aim of the present paper, however, was to develop a simple approximated approach to the fast abrasion model in order to extract simple analytical formulas for the most common physical observables. The results obtained, as compared with both the prediction of the extended abrasion model and with the experimental results, have revealed very satisfactory, especially when the analysis is restricted to impact parameters such that both the projectile and target abraded fragments have a mass less than or equal to half. The model has also been extended to include kinematical effects in order to obtain an analytical expression for angular and kinematical correlations between projectile-like and target-like fragments.

AKNOWLEDGMENTS

We like to thank Mr. F. Arriva for carefull drawings and Mrs. M. Ippolito for the typewriting of the manuscript.

REFERENCES

1) J. Barrette, B. Berthier, E. Chavez, O. Cisse, R. Dayras, R. Legrain, M.C. Mermaz, A. Pagano, E. Pollacco, H. Delagrange, W. Mittig, B. Heusch, G. Lanzanò and A. Palmeri, Proc. 22nd Int. Meeting on Nuclear Physics, Bormio (Italy), January 23 - 27, 1984.

2) J. Hüfner, K. Schäfer and B. Schürmann, Phys. Rev. C12 (1975) 1888 .

3) D.J. Morrissey, W.R. Marsh, R.J. Otto, W. Loveland and G.T. Seaborg,, Phys. Rev. C18 (1978) 1267; L.F. Oliveira. R. Donangelo and J.O. Rasmussen, Phys. Rev. C19 (1979) 826.

4) R. Dayras, A. Pagano, J. Barrette, B. Berthier, D.M. De Castro Rizzo, E. Chavez, O. Cisse, R. Legrain, M.C. Mermaz, E.C. Pollacco, H. Delagrange, W. Mittig, B.Heusch, R. Coniglione, G. Lanzanò and A. Palmeri, Nucl. Phys. A 460 (1986) 299., and R. Dayras et al. to be published.

5) J.D. Bowman, W.J. Swiatecki and C.F. Tsang, Lawrence Berkeley Laboratory Report N. LBL - 2908, 1973 unpublished.

6) W.J. Swiatecki, Report, 1976 (unpublished).

7) J. Gosset, H.H. Gutbrod, W.G. Meyer, A.M. Poskanzer, A. Sandoval, R. Stock and G.D. Westfall, Phys. Rev. C16 (1977) 629.

8) R. Coniglione, Tesi di Laurea, Universitã di Catania, 1983 (unpublished).

9) D. Guerreau, V. Borrel, D. Jacquet, J. Galin, B. Gatty and X. Tarrago, Phys. Lett. 131B (1983) 293.

10) F. Rami, Thèse d'Etat , Universitè de Strasbourg, 1985 (unpublished).

11) F. Gadi et al., to be published.

12) V. Borrel, These 3e cycle, Orsay 1984 (unpublished).

13) V. Borrel, B. Gatty, D. Guerreau, J. Galin, D. Jacquet, Report IPNO - DRE - 86/02.

14) Gomez del Campo, J. et al., Bull. Am. Phys. Soc. 30 (1985) 1283 and to be published.

15) A. Weidinger, F. Bush, G. Gaul, W. Trautmann, W. Zipper, Nucl. Phys. A263 (1976) 511 - 532.

16) A.S. Goldhaber, Phys. Lett. 53B (1974) 306.

17) R. Coniglione, G. Lanzanò, A. Pagano, J. Barrette, B. Berthier, D.M.C. Castro Rizzo, O. Cisse, R.A. Dayras, R. Legrain, M.C. Mermaz, H. Delagrange, W. Mittig and B. Heusch, Nucl. Phys. A447 (1986) 95c.

18) G. Lanzanò, A. Pagano, R. Dayras, R. Coniglione, J. Barrette, B. Berthier, D.M.C. De Castro Rizzo, O. Cisse, R. Legrain, M.C. Mermaz, H. Delagrange, W. Mittig, B. Heush, Proc. of the XXIV Intern. Winter Meeting on Nuclear Physics, Bormio (Italy) January 1986.

19) R. Dayras et al. to be published.

20) R. Dayras, Journal de Physique, Colloque C4, Suppl. N. 8, Tome 47, pag. 13 (1986).

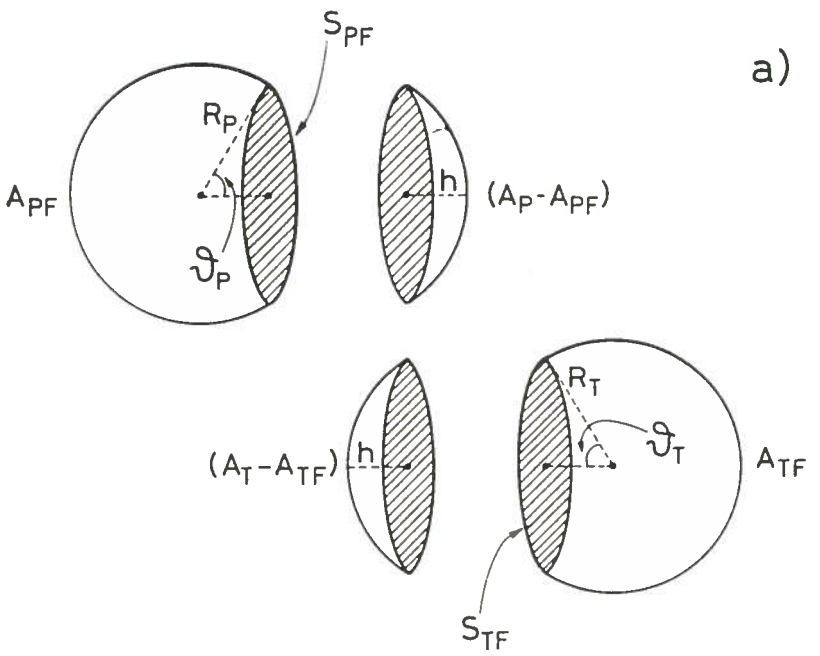

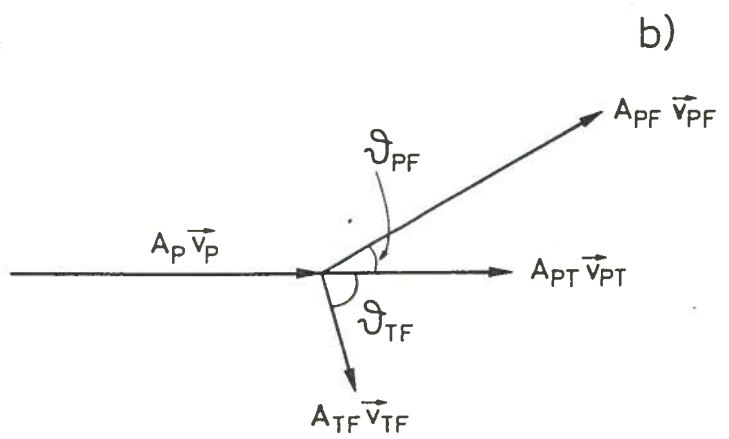

Fig.1. a) Sketch showing the simplified fast abrasion mechanism. A_{PF} and A_{TF} are the masses of the projectile and target spectators respectively, while $(A_P - A_{PF})$ and $(A_T - A_{TF})$ are the masses of the projectile and target participants respectively. The projectile and target abraded surfaces S_{PF} and S_{TF} are supposed flat.

b) Kinematical sketch showing the momenta involved in the ingoing and autgoing reaction channel in the Laboratory system.

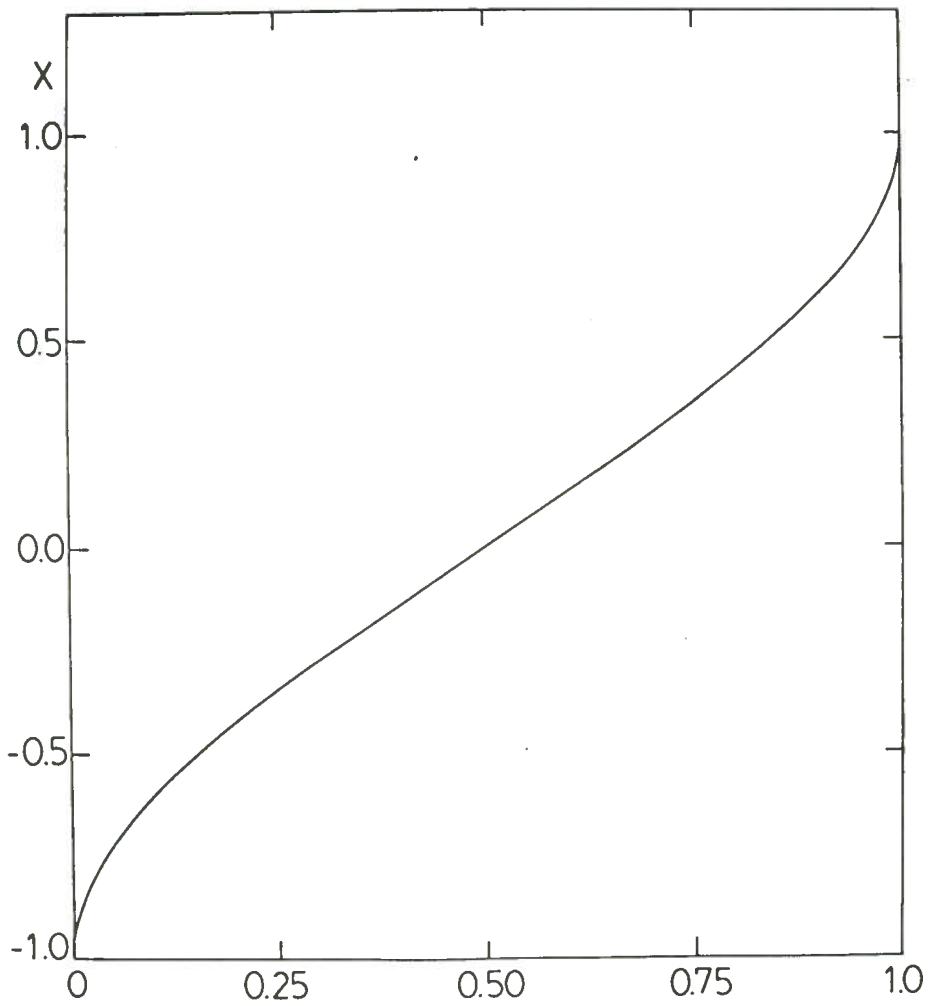

Fig.2. The "reduced impact parameter" $x=\cos\theta_p$ against the projectile-like fragment mass A_{PF} (normalized to the projectile mass A_p).

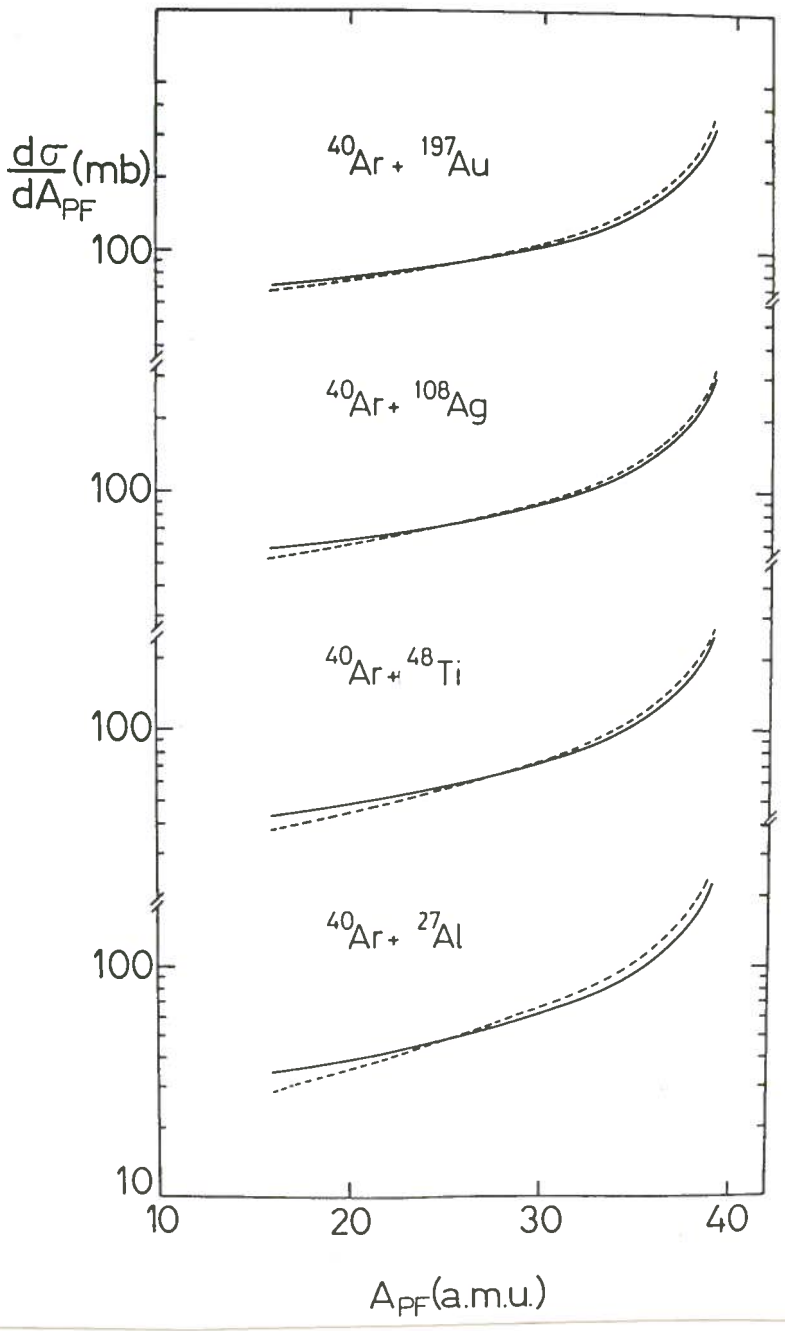

Fig.3. Mass yield for the production of projectile-like fragments in reactions induced by an ^{40}Ar beam on various target. Continuous and broken curves are the result of the present and the extended abrasion model respectively.

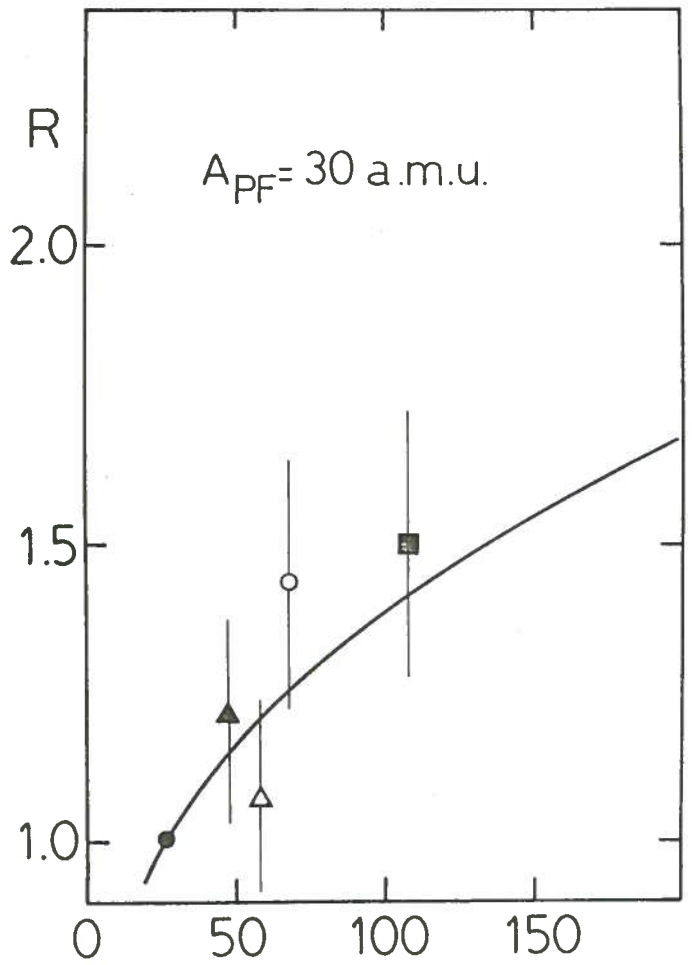

Fig.4 Production of the projectile-like fragment mass A_{PF}=30 as a function of the target mass A_T for reaction induced by an ^{40}Ar beam on various targets at intermediate energies. The data are normalized to the value of 70 mb relative to the reaction $^{40}Ar+^{27}Al$ at 44 MeV/u. The experimental points refer to the following reactions:

● $^{40}Ar+^{27}Al$ 44 MeV/u ref. [1,4]

▲ $^{40}Ar+^{nat}Ti$ 44 MeV/u ref. [1,4,8]

△ $^{40}Ar+^{58}Ni$ 44 MeV/u ref. [9]

○ $^{40}Ar+^{68}Zn$ 27 MeV/u ref. [10]

■ $^{40}Ar+^{nat}Ag$ 30 MeV/u ref. [11]

The solid line is obtained by using equation (7) of the text, with A_{TO}=27 and A_P=40.

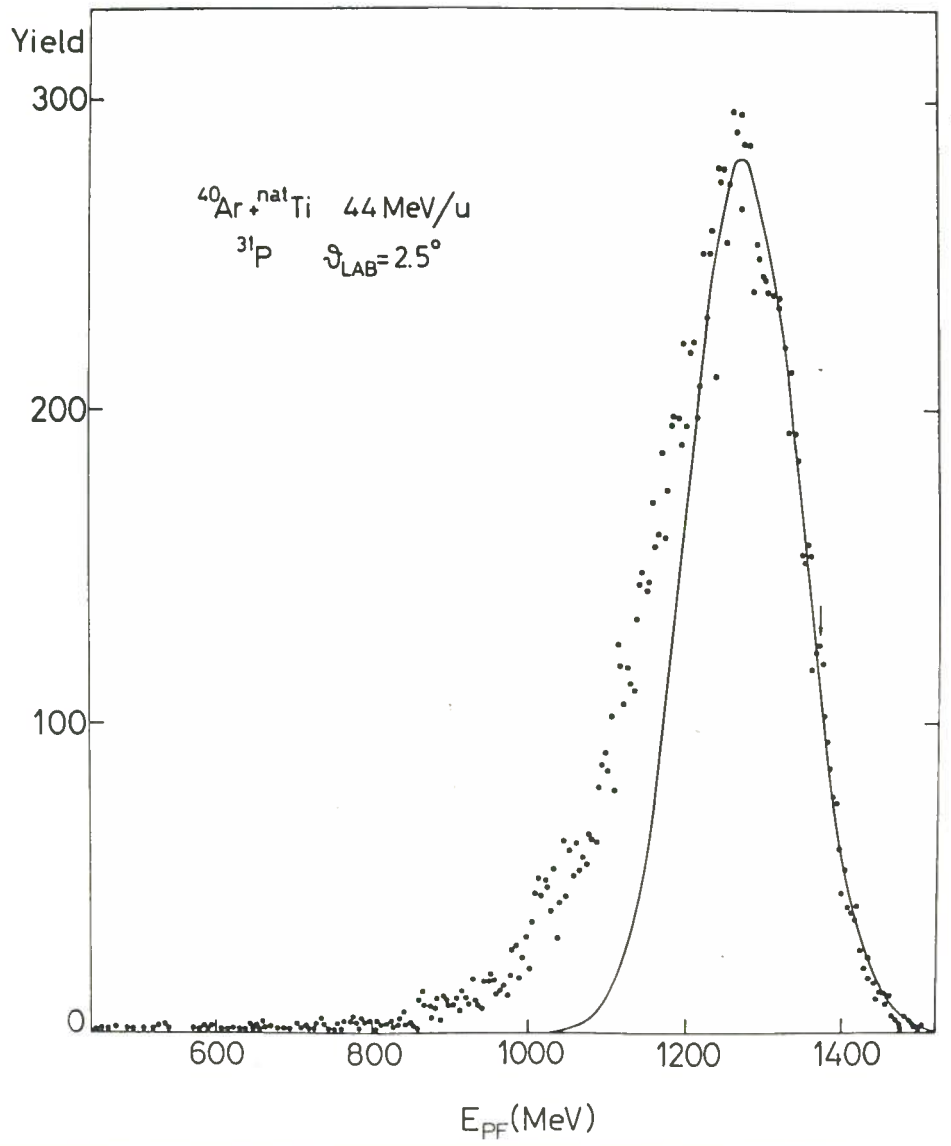

Fig.5 The energy spectrum for the projectile-like fragment ^{31}P in the reaction $^{40}Ar + ^{nat}Ti$ at 44 MeV/u. The solid line has been obtained by fitting equ.(5) of ref.[4] to the high energy data of the spectrum (starting from 80% of the maximum). The arrow indicates the ^{31}P energy corresponding to a velocity equal to the beam velocity

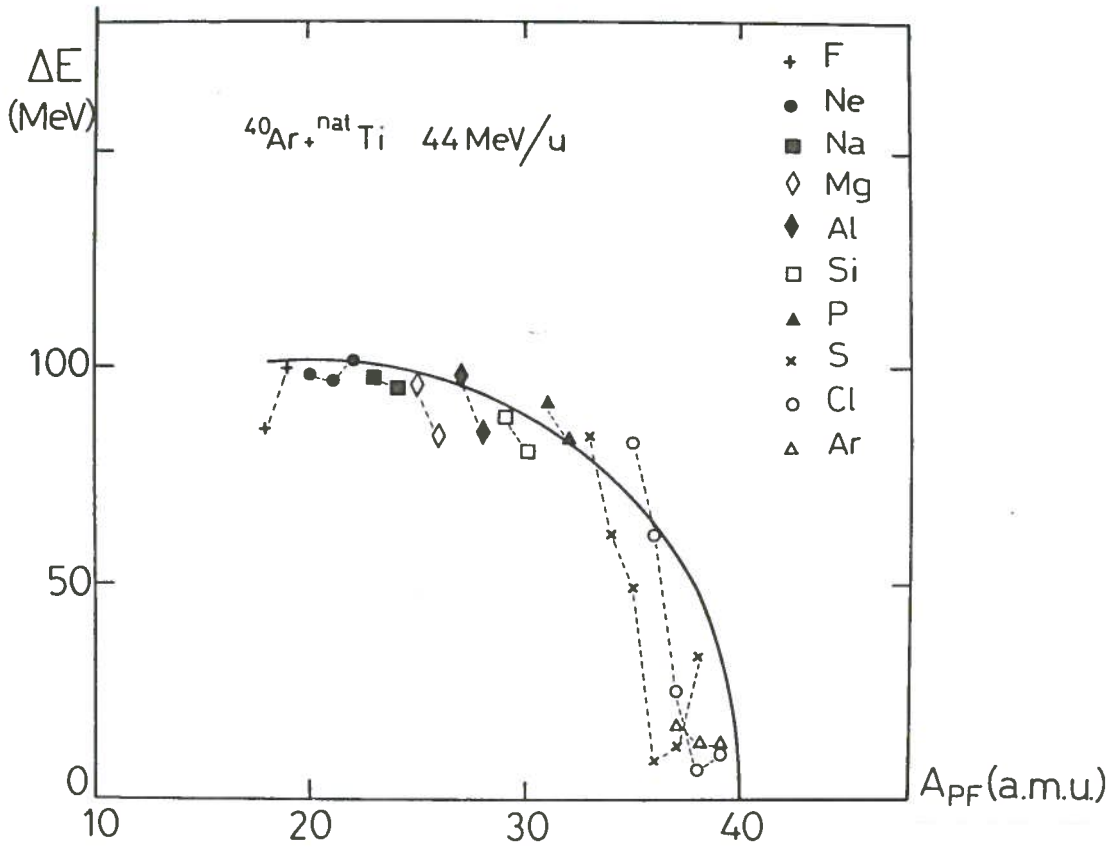

Fig.6 The energy shift (equ.(8)of the text) of the projectile-like fragments against their mass. The solid line is obtained by using equ.(8)with r_0=1.2 fm.

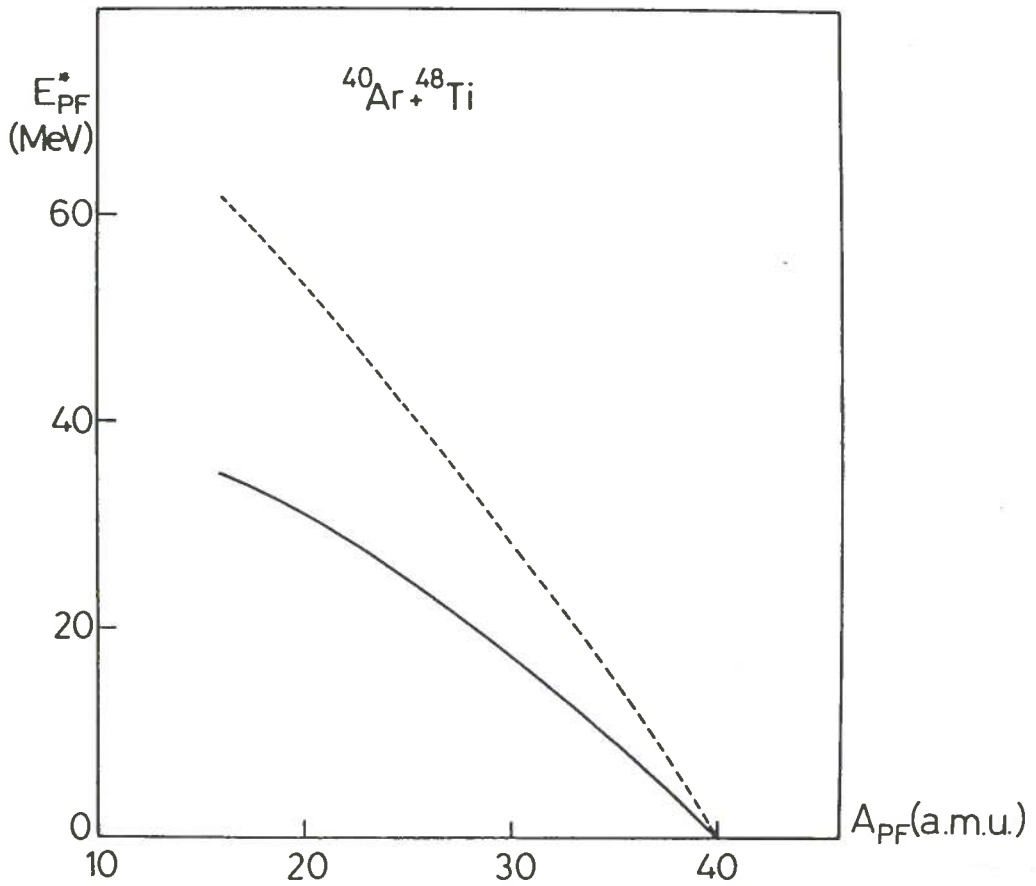

Fig.7 The excitation energy of the proiectile-like fragments against their mass. Solid and dashed lines refer to the present and to the extended abrasion model respectively.

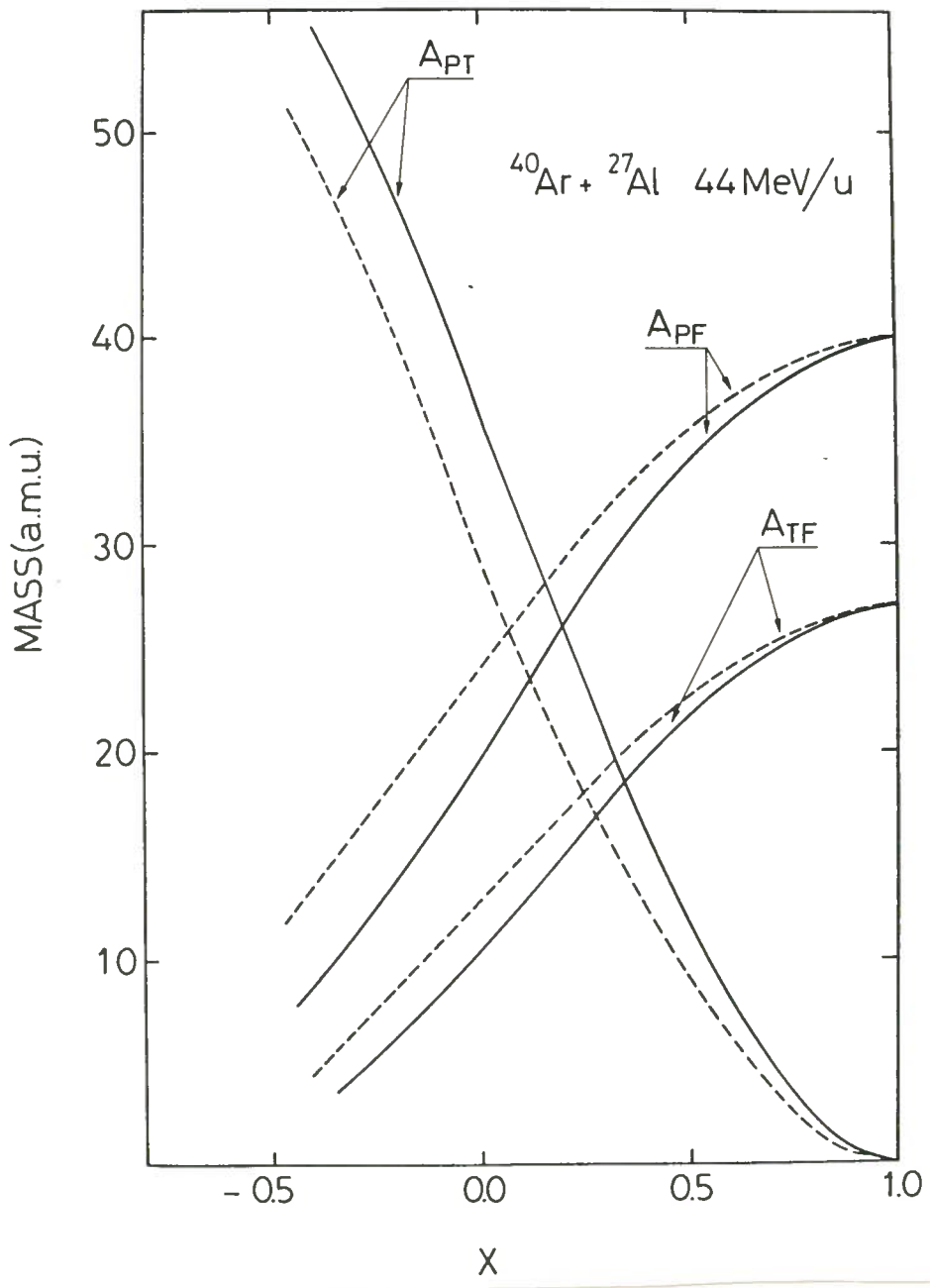

Fig.8 The mass of the participants A_{PT}, of the projectile-like fragments A_{PF} and of the target-like fragments A_{TF} as a function of the "reduced impact parameter" x. Solid and dashed lines refer to the present and to the extended abrasion model respectively.

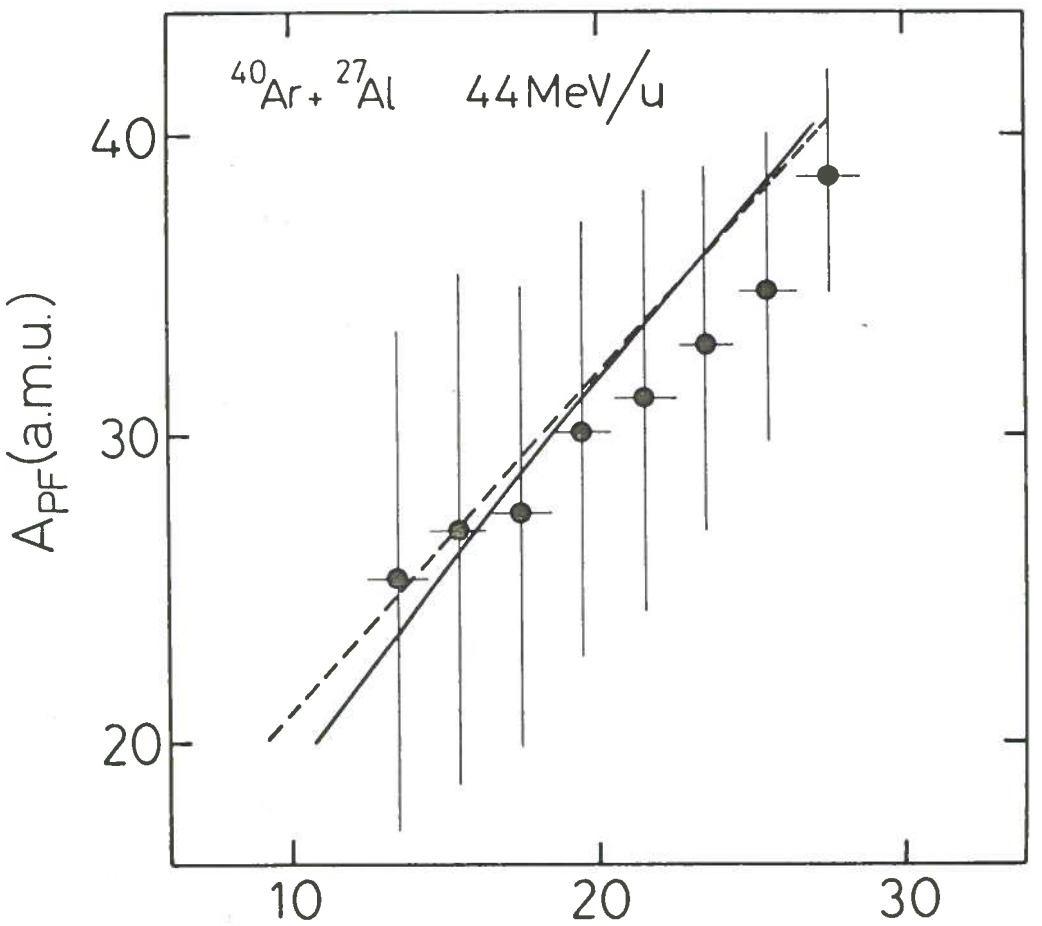

Fig.9 The mass-mass correlation function for the projectile-like fragments and the target-like fragments. The solid and dashed curves are the predictions of the present and the extended abrasion model respectively. Experimental points from ref.[17].

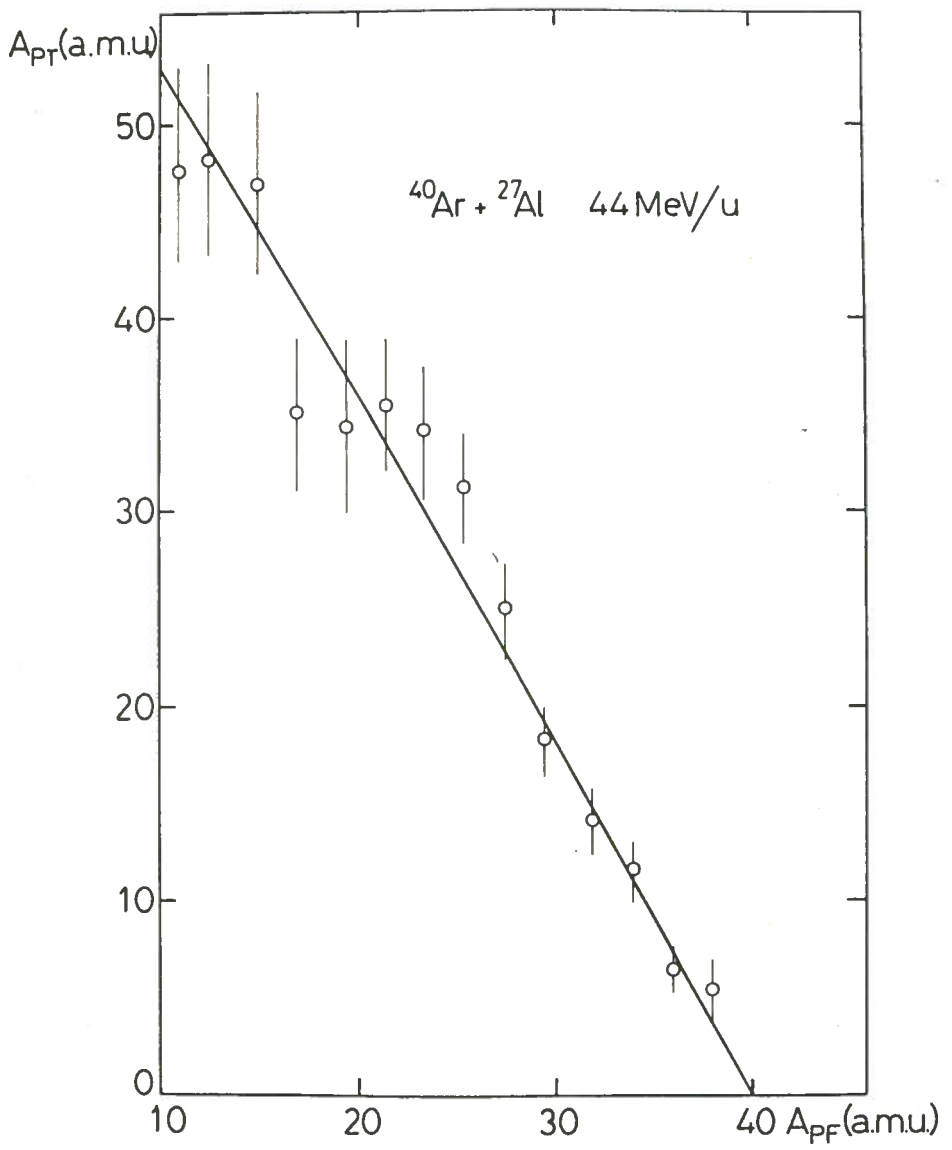

Fig.10 The mass-mass correlation function for the participants and the projectile-like fragments (equ.(16),solid line). The experimental points (arbitrarily normalized) represent the α particles differential multiplicity at +25° in coincidence with the projectile-like fragments detected at +3.1° for the reaction $^{40}Ar+^{27}Al$ at 44 MeV/u, as a function of the projectile-like fragment mass A_{PF}.

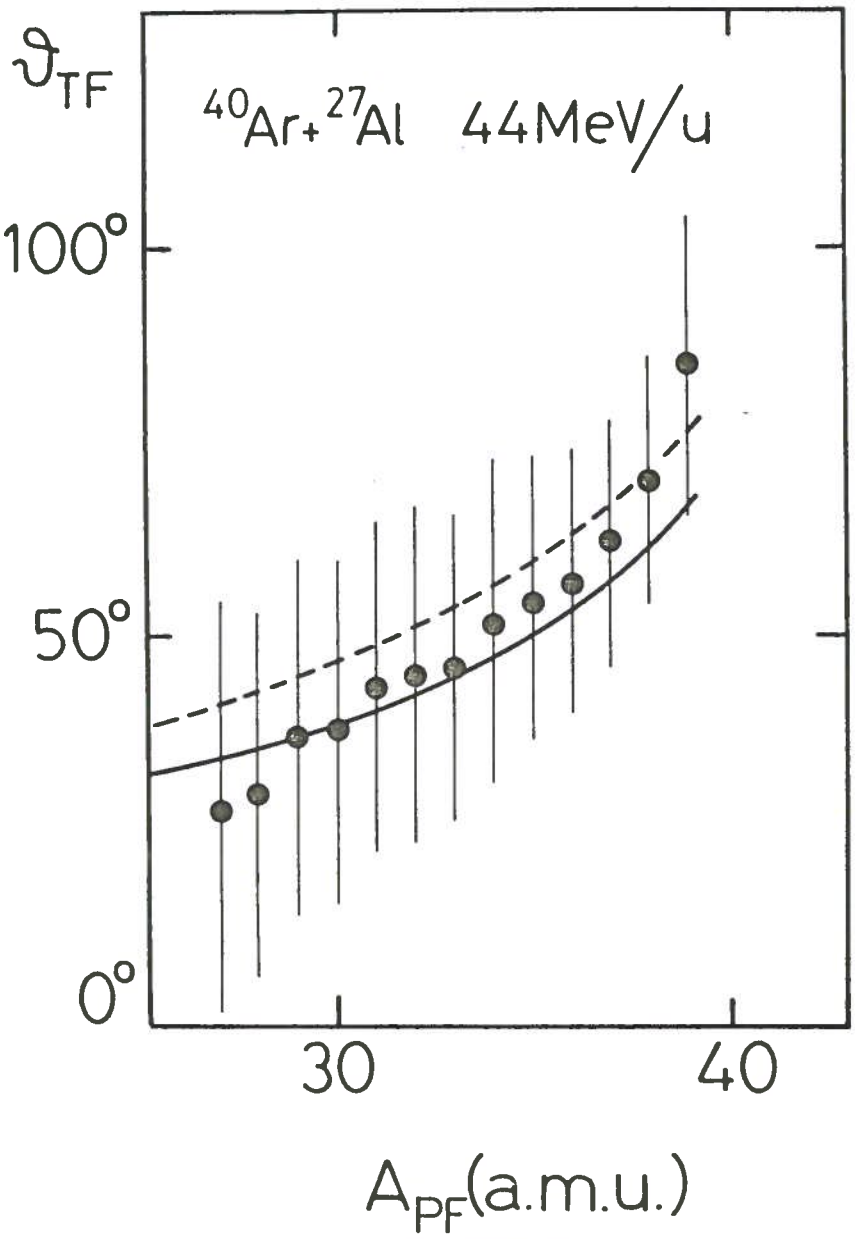

Fig.11 The recoiling angle θ_{TF} of the target-like fragment against the coincident projectile-like fragment mass A_{PF}, for the reaction $^{40}Ar+^{27}Al$ at 44 MeV/u ref.[17]. Solid and dashed curves are the prediction of the present and the extended abrasion model respectively.